International Journal of Nanomedicine

Dovepress
open access to scientific and medical research

Open Access Full Text Article

ORIGINAL RESEARCH

The Pharmacological Effects of Silver Nanoparticles Functionalized with Eptifibatide on Platelets and Endothelial Cells

Justyna Hajtuch[1], Eliza Iwicka[1], Anna Szczoczarz[1], Damian Flis[1], Elżbieta Megiel[2], Piotr Cieciórski[2], Marek Witold Radomski[3], Maria Jose Santos-Martinez[4], Iwona Inkielewicz-Stepniak[1]

[1]Department of Pharmaceutical Pathophysiology, Medical University of Gdansk, Gdansk, Poland; [2]Faculty of Chemistry, University of Warsaw, Warsaw, Poland; [3]Department of Anatomy, Physiology and Pharmacology, University of Saskatchewan, Saskatoon, Saskatchewan, Canada; [4]School of Pharmacy and Pharmaceutical Sciences and School of Medicine, Trinity College Dublin, Dublin, Dublin 2, Ireland

Correspondence: Iwona Inkielewicz-Stepniak, Tel +48 58 349 1516, Fax +48 58 349 1517, Email iwona.inkielewicz-stepniak@gumed.edu.pl

Purpose: In the search for new drug delivery platforms for cardiovascular diseases and coating of medical devices, we synthesized eptifibatide-functionalized silver nanoparticles (AgNPs-EPI) and examined the pharmacological activity of AgNPs-EPI on platelets and endothelial cells in vitro and ex vivo.

Methods: Spherical AgNPs linked to eptifibatide were synthesized and characterized. Cytotoxicity was measured in microvascular endothelial cells (HMEC-1), platelets and red blood cells. Platelet mitochondrial respiration was measured using the Oxygraph-2k, a high-resolution modular respirometry system. The effect of AgNPs-EPI on the aggregation of washed platelets was measured by light aggregometry and the ex vivo occlusion time was determined using a reference laboratory method. The surface amount of platelet receptors such as P-selectin and GPIIb/IIIa was measured. The influence of AgNPS-EPI on blood coagulation science was assessed. Finally, the effect of AgNPs-EPI on endothelial cells was measured by the levels of 6-keto-PGF1alpha, tPa, cGMP and vWF.

Results: We describe the synthesis of AgNPs using eptifibatide as the stabilizing ligand. The molecules of this drug are directly bonded to the surface of the nanoparticles. The synthesized AgNPs-EPI did not affect the viability of platelets, endothelial cells and erythrocytes. Preincubation of platelets with AgNPs-EPI protected by mitochondrial oxidative phosphorylation capacity. AgNPs-EPI inhibited aggregation-induced P-selectin expression and GPIIb/IIIa conformational changes in platelets. AgNPs-EPI caused prolongation of the occlusion time in the presence of collagen/ADP and collagen/adrenaline. AgNPs-EPI regulated levels of 6-keto-PGF1alpha, tPa, vWf and cGMP produced in thrombin stimulated HMEC-1 cells.

Conclusion: AgNPs-EPI show anti-aggregatory activity at concentrations lower than those required by the free drug acting via regulation of platelet aggregation, blood coagulation, and endothelial cell activity. Our results provide proof-of-principle evidence that AgNPs may be used as an effective delivery platform for antiplatelet drugs.

Keywords: drug delivery, antiplatelet, RGD, aggregation, coagulation system, biocompatibility

Introduction

Hemostasis is a tightly regulated process that ensures vascular integrity. Following accidental vascular injury, the hemostatic system initiates vascular events, restores the hemostatic balance, and prevents a pathological extension of hemostasis, ie, thrombosis.[1] Hemostasis acts as an interplay between blood platelets, coagulation and fibrinolysis proteins, and endothelial cells. The endothelium was originally thought to be a simple passive barrier between the intravascular and extravascular compartment but is now viewed as an organ whose function is critical to maintaining hemostasis and promoting vascular health. The most important endothelial functions include regulation of vascular tone, cell adhesion, smooth muscle cell proliferation, and vascular wall inflammation. In addition, the endothelium serves as a hemocompatible lining that helps maintain blood flow and blood regulation coagulation system.[2] Endothelial cells secrete antiplatelet and anticoagulant agents that prevent platelet aggregation and fibrin formation. Endothelial dysfunction occurs due to a pathological process, which

Received: 11 May 2022
Accepted: 4 August 2022
Published: 19 September 2022

Graphical Abstract

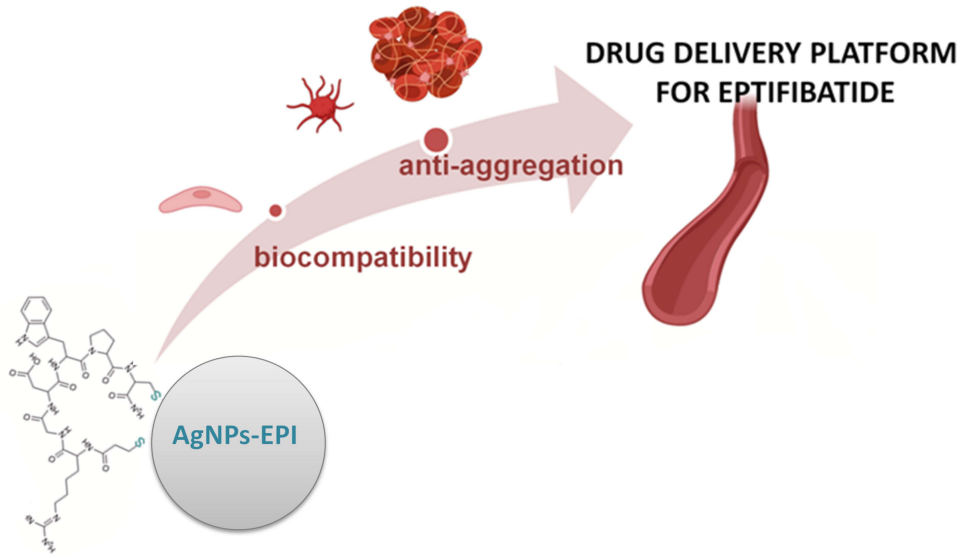

may lead to increased platelet adhesion, aggregation, fibrin generation, and formation of occlusive thrombi.[3] Intact endothelium inhibits platelet adhesion by releasing nitric oxide and prostaglandin I_2, while activated endothelial cells secrete various molecules and receptors that increase platelet adhesion and aggregation to the injury site.[4] Thrombocytes play a significant role in the process of primary haemostasis, during which the platelet plug forms. It begins with the adhesion of platelets to the point where the continuity of a blood vessel has been broken. As a result of the injury, collagen fibers are exposed, with which the Ib/V/IX receptor complex present on the surface of blood platelets binds. The adhesion of platelets to the injured endothelium is also enhanced by the participation of von Willebrand factor, which forms a bond with glycoprotein Ib. Platelets adjacent to the site of damage are simultaneously activated, which leads to degranulation and the release of biologically active substances stored in granules.[5] Platelet aggregation is the major pathophysiological factor in the development of arterial ischaemic events, including coronary artery disease, cerebrovascular accidents, peripheral arterial disease.[6] Moreover, platelet activation and dysfunction have been implicated in diabetes, renal diseases, tumorgenesis, Alzheimer's, and cardiovascular diseases (CVD). CVD is the leading cause of death worldwide and encompasses diverse pathologies, including coronary heart disease, cerebrovascular disease, deep vein thrombosis, and pulmonary embolism.[7] The vascular therapy with antiplatelet agents is the cornerstone of clinical management of CVD. The way of antiplatelet therapy has changed over the past decade with the advent of several new drugs with different mechanisms of action.[6]

Eptifibatide is a synthetic cyclic heptapeptide deriving from the venom of southeastern pygmy rattlesnake that reversibly binds to platelet GPIIb/IIIa receptor resulting in a short-lasting receptor blockade and inhibition of platelet aggregation. In addition to tirofiban and abciximab, it belongs to the group of drugs that bind reversibly to the platelet GPIIb/IIIa receptor, causing short-term blockade of the receptor and inhibition of platelet aggregation. The compound also relaxes the coronary artery through endothelial-dependent NO-cGMP signaling. Blockade of platelet GPIIb/IIIa with eptifibatide has improved endothelial-dependent vasodilation.[8,9] The available studies suggest that eptifibatide is more safe than tirofiban in patients with acute coronary syndrome. The data also show that it increases survival during percutaneous coronary intervention compared to abciximab.[10,11] The major rate-limiting factor for the pharmacological use of EPI is its short half-life due to accumulation in non-targeted tissues and elimination by renal filtration. Advances in nanomedicine led to the pharmaceutical design of drug delivery platforms using nanoparticles allowing for controlled and targeted drug administration.[12,13] Silver nanoparticles (AgNPs) are an attractive tool for drug delivery platforms. Indeed, AgNPs can be functionalized in a specific way with molecular encapsulating agents such as proteins and ligands

connected via chemical bonds. In the last case, the synthesized nanoparticles exhibit high stability and tunable releasing of the bioactive ligands under the influence of the environment.[14] Especially beneficial is the connection via the Ag-S bond (thiolate bond) because it gives a possibility to obtain stable nanoparticles that can be separated in a solid-state and detailed characterized. Furthermore, such a form of potential pharmaceutics offers a broader range of drug preparation. This type of drug connection with the nanoparticle's surface is possible if the ligand contains mercaptyl or disulfide groups in its molecules. In the case of eptifibatide, disulfide groups in its molecules enable the connection directly to the silver surface without any linker. Noteworthy, the AgNPs show a strong antibacterial effect that improves infection treatment[15–17] Our recent studies have shown that the functionalized AgNPs synthesized by our team can inhibit platelet aggregation under flow conditions by reducing the expression of P-selectin and GPIIb/IIa receptors.[18] This paper reports the synthesis of narrow-dispersive, stable silver nanoparticles linked directly with eptifibatide molecules (AgNPs-EPI) via thiolate bonds. We also studied the impact of AgNPs-EPI on thrombin-induced endothelial dysfunction.[19,20] Our results indicate that AgNPs-EPI acts as a new inhibitor of platelet and endothelial cell activation and could be used as a platform for drug delivery in cardiovascular diseases and for coating medical devices.

Materials and Methods

Nanoparticle Synthesis and Characterization

30 mg of eptifibatide (EPI) was dissolved in 30 mL of H_2O and transferred to the flask immersing in an ice-water bath on a magnetic stirrer. After 15 minutes of stirring, 24 µL of 1 M $AgNO_3$ was added, and the mixture was stirred for the next 15 minutes; while stirring, the flask was covered with aluminum foil protecting against light. Next, 110 mg of $NaBH_4$ dissolved in 16 mL H_2O and cooled down in a fridge was added drop by drop. The mixture became first yellow, light brown, and finally dark brown during the addition of the reducing agent. The mixture was stirred for four h at room temperature. Protected against the light. Afterward, the solution was transferred to a dialysis bag, purified from inorganic compounds, and EPI molecules not connected with the NP's surface against ultrapure water for 48 h (the dialysate was changed three times). AgNPs were characterized by transmission electron microscopy (TEM), UV-vis spectrophotometry, thermogravimetric analyses (TGA), dynamic light scattering (DLS), transform infrared (FTIR) and zeta potential measurements. UV–vis absorption spectra were recorded using a Cary 50 UV/Vis spectrophotometer in ultra-pure water in the 200–800 nm range with a 1 cm quartz cell. Thermogravimetric analyses (TGA) were performed under N_2 using Q50-1261 TA Instruments (USA) with temperature compensated thermobalance (precision ±0.01%), a heating rate of 10 $K \cdot min^{-1}$. Weight loss during thermal decomposition was determined in the temperature range of 20–1000°C. Transmission electron microscopy (TEM) observations have been carried out using JEM 1400 JEOL Co. microscope at 120 kV acceleration voltage. The samples were obtained by casting the water solution of materials onto a carbon-coated copper microgrid (200 mesh) and air-dried overnight. Dynamic Light Scattering (DLS) measurements were performed with a Zetasizer Nano series apparatus (Malvern) with a backscattering detection at a constant 173 scattering angle equipped with a He-Ne laser (4 mW) at 632.8 nm using a thermostated cell holder. The hydrodynamic diameters of the particles were measured at 25°C, and size distribution by number was determined in ultra-pure water. The surfaces' potential zeta (ζ-potential) was determined for the same solution as hydrodynamic diameter measurements using Zetasizer folded capillary cells for electrophoresis. Fourier transform infrared (FTIR) spectroscopy measurements were performed on a Shimadzu FT-IR model 8400S spectrophotometer. FTIR spectra (absorption mode) were recorded with a resolution of 4 cm^{-1} from KBr pellets in a ratio of 1:1000 (w/w) in the case of AgNPs-EPI and 1:300 (w/w) for EPI. All compounds used in our studies show a purity >97%, determined by HPLC analyses. Eptifibatide acetate (≥98%, HPLC), silver nitrate (ACS reagent, ≥99%), sodium borohydride (≥98%), Milli-Q ultrapure water (resistivity 18.2 MΩ cm^{-1}, Millipore-Merk) was used in all the experiments. Dialysis cellulose membranes (Nadir, Bionovo) with molecular weight cut-off (MWCO) 10,000 Da were used to purify the synthesized nanoparticles.

Cell Culture

Immortalized human microvascular endothelial cell line (HMEC-1) were obtained from the ATCC (CRL-3243) and maintained as a monolayer culture in T-75 cm^2 tissue culture flasks. HMEC-1 cells were cultured in an MCDB131 medium (Life Technologies, cat# 10372019) in the presence of 6 µg/mL penicillin-G and 10 µg/mL streptomycin (Pan_Biotech, P06-07100).

Cells were cultured at 37°C in a humidified atmosphere containing 5% CO_2. When confluent, cells were detached with trypsin-EDTA (Merck, T4049) and sub-cultured into a new cell culture flask. The medium was replaced every second day.

Incubations of Endothelial Cells with AgNPs-EPI, AgNPs, and Eptifibatide

For all cellular experiments, HMEC-1 cells were incubated in the presence of experimental agents for the time described in each method. Concentrations used in those experiments were selected from preliminary studies. AgNPs-EPI or AgNPs were diluted in FBS-free media and shaken well to ensure equal dispersion of NPs in the solution. In some experiments, eptifibatide acetate (Merck SML1042) was used at the concentration corresponding to the drug content in AgNPs-EPI to measure the effects of the free drug. Control cells were treated with NPs-free and FBS-free culture media.

Blood Collection and Platelet Isolation

The Bioethics Committee approved the study of the Medical University of Gdansk (NKBBN/552/2018–2021). It was also performed in accordance with the Code of Ethics of the World Medical Association, the ethical standards of the competent commission for Human Experiments (institutional and national), and the Helsinki Declaration of 1975 r., as amended in 2000. Blood was withdrawn from healthy volunteers who had not taken any drug known to affect platelet function for at least two weeks prior to the study. Each volunteer signed an informed consent form, had sufficient time to read the consent, and received comprehensive answers to the questions asked. For LDH assay, light aggregometry, and flow cytometry, whole blood was collected using 3.15% tri-sodium citrate (9:1, v:v). Washed platelet (WP) suspensions were isolated from blood as described by Radomski and Moncada and suspended using Tyrode's solution at the final concentration of 250,000 platelets/μL.[21] For mitochondria respiration experiments, platelets were prepared as previously described.[22] For coagulation studies, 3 mL of blood was collected using 3.8% buffered sodium citrate and prepared according to the reference recommendations for each method.

MTT Viability

HMEC-1 were seeded in 96-well plates (15,000 cells per well) with complete media. After 24 h, media was removed from the wells, and cells co-incubated with NPs at concentrations ranging from 0.5 to 150 μg/mL for AgNPsEPI. After 24 h, the media was supplemented with water-soluble tetrazolium salt (at a final concentration of 0.5 μg/mL) and incubated for two h. Next, the media was removed, and the resultant crystals dissolved in DMSO. After 15 min, cell viability was studied by measuring absorbance at 490 nm using a microplate reader (Synergy H1, BioTek). Viability was determined as a percentage of the control where the viability of control cells was set as 100%. Absorbance values were corrected with blank NPs.

Lactate Dehydrogenase (LDH) Release

The cytotoxic effect of AgNPs-EPI was measured by detecting LDH release following exposure of WP to AgNPs-EPI (10–150 μg/mL) at 37°C for 20 min by using a Cytotoxicity Detection LDH kit (Promega, Poland), according to the manufacturers' instructions. WP treated with lysis buffer (0.1% Triton X-100) was used as a positive control (total LDH release). Lysis buffer-treated cells were set to 100%. AgNPs-EPI was used as a background control, and their absorbance was subtracted from the reading of the samples. Results are given as % of the total LDH release from the cells. Absorbance was measured at 490 nm using a microplate reader (Synergy H1, BioTek).

Analysis of Hemolytic Properties of AgNPs-EPI

To assess the effect of AgNPs-EPI on RBCs, peripheral blood was collected into a syringe containing sodium citrate (0.35% final conc.) and 10 mL centrifuged at 300 xg for 10 min at room temperature. Platelet rich plasma and buffy coat were removed by aspiration and the red blood cells (RBCs) were diluted in PBS (1:100), plated in 96-wells and co-incubated with AgNP-EPI for 12 h. Hemolysis was determined by measuring hemoglobin. Absorbance was recorded at 540 nm for hemoglobin, using a microplate reader (Synergy H1, BioTek). Data expressed as % of hemoglobin release, 0.1% Triton X −100 (Sigma-Aldrich, St. Louis, MO) was used as the positive control. One hundred percent lysis was corroborated by optical microscope.

Platelet Function

To measure platelet aggregation under stirring, the response of platelets to collagen (2 μg/mL) in WP was tested using light aggregometry. Briefly, WP samples (2.5×10^8 cells/mL) were placed in a two-channel aggregometer (CHRONO-LOG-700) and incubated for 20 mins at 37°C, stirring at 900 r.p.m. in the presence or absence of AgNPs-EPI or EPI. Collagen (2 μg/mL) was added to the incubating, and the extent of aggregation was measured for 20 mins. To measure flow-induced platelet aggregation, in the presence or absence of AgNPs-EPI (50 μg/mL), the Innovate PFA-200 system (Siemens Healthcare Diagnostics Products, Munich, Germany) was used.

Flow Cytometry

The abundance of P-selectin and activated GPIIb/IIIa on the surface of platelets in the presence of AgNPs-EPI and EPI (25 and 50 μg/mL) was detected by flow cytometry. Collagen (2 μg/mL) induced platelet aggregation in WP was used as a positive control, whereas WP without collagen (resting platelets) was used as a negative control. Platelets in WP were pre-incubated with AgNPs-EPI and EPI (25 and 50 μg/mL) for 20 mins before adding collagen (2 μg/mL). Then, samples were collected and incubated in the dark for 15 mins at room temperature in the presence of 10 μg/mL of P-selectin (CD62P) and integrin GPIIb/IIIa (CD41/CD61) antibody (BioLegends, 304902 and 362803), respectively. Subsequently, samples were diluted in Tyrode's solution and analyzed using a BD FACS (Calibur). Platelets were identified by forward and side scatter signals, and the flow cytometer analyzed 10,000 platelet-specific events for fluorescence. The obtained data were analyzed using CellQuest software.

6-Keto-PGF1alpha, tPa, vWF and cGMP Levels

6-keto-PGF1alpha (a stable metabolite of prostacyclin), tissue plasminogen activator (tPa), von Willebrand factor (vWF), and cyclic guanosine monophosphate (CGMP) levels were measured in cell culture medium or cell lysate by commercially available enzyme linked immunosorbent assays (Abcam and BioFine). Cells were plated onto a 6-wells plate and incubated overnight. AgNPs-EPI and EPI were used at concentrations of 25 and 50 μg/mL. After 24h, Thrombin (Sigma Aldrich, T4393) was added to some of the wells (2U/mL for 1 hour) as a stimulator of endothelial dysfunction. Next, media were collected, aliquoted, and stored at −80°C. Cells were lysed in a lysis buffer containing protease inhibitors. The cell lysate was aliquoted and stored at −80°C. All tests were performed according to the manufacturer's protocols. The absorbance associated with samples, standard curves, and negative controls was measured using a Synergy H1 microplate reader (Biotek) at 450 nm with a wavelength correction of 540 nm.

High-Resolution Respirometry

Washed platelets (300 000 per each 2 mL chamber) were resuspended in MiR05 (mitochondrial respiration medium containing 0.5 mM EGTA), 3 mM MgCl2·6H2O, 60 mM potassium lactobionate, 20 mM taurine, 10 mM KH2PO4, 20 mM HEPES, 110 mM sucrose, and 1 g/L fatty acid BSA-free (pH 7.1). Mitochondrial respiration was measured in a high-resolution respirometer using an Oxygraph-2k (O2k, Oroboros Instruments, Innsbruck, Austria), a modular system for high-resolution respirometry (HRR). Platelet samples were incubated at 37°C under constant stirring (750 rpm), ensuring a medium's homogenous oxygen distribution. Respiration of permeabilized platelets was determined using substrate-uncoupler inhibitor titration (SUIT) protocol as previously described.[23,24] After normal respiration was established, platelets were preincubated for 10 min in the presence or absence of AgNPs-EPI (50 μg/mL) or EPI (50 μg/mL). Following preincubation, collagen (2 μg/mL) was added to activate platelets. After another 5 min of incubation, titration was started with permeabilization of the cells with digitonin (10 μg/mL) and the addition of NADH-related substrates: pyruvate, glutamate, and malate (5 mM, 5 mM, and 0.5 mM, respectively) to induce leak respiration (state L). OXPHOS capacity of complex I (state CI) was evaluated by adding ADP (2.5 mM). Next, succinate (10 mM) was added to obtain maximal OXPHOS capacity with convergent input through complex I and II (state CI + CII). Oligomycin (1 μg/mL) was used to inhibit the ATP synthase. Titrations with the uncoupler FCCP (0.5 μM steps) were performed to determine electron transfer system (ETS) capacity (state E). Rotenone (0.5 μM, the inhibitor of complex I of ETS, state R) and Antimycin-A (2.5 μM, the inhibitor of to inhibit complex III of ETS) were added for determination of residual

oxygen consumption (ROX). Oxygen concentration (μM) and oxygen flux [pmol $O2 \cdot s^{-1} \cdot 10^{-6}$ cells] were recorded in real-time while obtained data were evaluated using DatLab software (Oroboros Instruments, Innsbruck, Austria). The OXPHOS coupling efficiency was calculated to measure mitochondrial quality and control. OXPHOS coupling efficiency, calculated with the formula (1 − (state L)/(state CI + CII)), reflects the coupling of respiration supported by electron transferring flavoprotein (ETF) with pyruvate, glutamate, malate, and succinate as substrates after addition of ADP (state CI + CII) and state L. A lower value of OCE denotes lesser coupling of the oxidation and phosphorylation after the addition of ADP.

Blood Coagulation

Several tests were used to measure the impact of AgNPs-EPI (50 μg/mL, 2 hours of incubation time) on the activity of factors involved in the coagulation cascade. Aqua pro-Injectione (Polpharma, Stargard Gdanski, Poland) was used in control experiments. Plasma fibrinogen was measured using the modified Clauss method. The assay measures the ability of fibrinogen to form fibrin clots after being exposed to a high concentration of purified thrombin. Under such conditions, the clotting time depends primarily on the presence of fibrinogen in the sample. APTT (Activated partial thromboplastin time) reflects the activity of coagulation factors of the intrinsic and common pathway (XII, XI, IX, X, VIII, II, and I). The test is performed by incubating plasma with an appropriate amount of phospholipids and a contact activator. The addition of calcium ions triggers the clotting process; the time until fibrin formation is measured. APTT ratio is the ratio of a patient's APTT to the regular laboratory reference APTT. The Prothrombin time (PT) measures the integrity of the extrinsic and final common pathways of the coagulation cascade. The coagulation cascade is activated by incubating the plasma with an optimal amount of calcium and thromboplastin, an activator of the extrinsic pathway; the clotting time is then measured. PT ratio is the ratio of a patient's PT to the standard laboratory reference PT. INR is derived from prothrombin time (PT). It is calculated as a ratio of the patient's prothrombin time to the control prothrombin time standardized for the potency of the thromboplastin reagent. Antithrombin III is converted by heparin to a direct inhibitor that inactivates the thrombin present in the sample. A kinetic test determines the residual thrombin content; the absorbance measured at 405nm is inversely proportional to the activity of antithrombin III in the sample. Thrombin time (TT) measures the last step in the clotting cascade. Standardized thrombin concentration is added to plasma, and time to fibrin clot formation is measured. D – Dimers - polystyrene molecules covalently bound to monoclonal antibodies (8D3) aggregate upon mixing with D-dimers samples. An aggregation reaction is then detected turbimetrically due to the increased turbidity of the sample. All tests were performed at the accredited hospital laboratory using a BCS-XP analyzer (Siemens Healthcare, Marburg, Germany).

Statistical Analysis

Each experiment was replicated independently three times. Data are presented as mean ± standard deviation (SD). Statistical analysis was performed using Prism 5 software (GraphPad), the one-way analysis of variance (ANOVA), and Tukey's post hoc test.

Results

Nanoparticle Synthesis and Characterization

The conjugate AgNPs-EPI has been synthesized via the chemisorption of eptifibatide molecules onto a silver surface. In this process, silver nitrate was used as a source of silver ions, sodium borohydride as a reducing agent and eptifibatide as a stabilizing ligand. The reaction was carried out at a low temperature (around 4°C) to obtain nanoparticles with narrow size distribution.

Figure 1 shows the spectra recorded during the synthesis and purification steps of AgNPs-EPI. Namely, after adding the reducing agent, when the reaction was stopped (4h), after the dialysis process (20h), and the final product after 48 h of dialysis was dispersed in water. The position of the maximum Surface Plasmon Resonance (SPR) band in the UV-vis spectrum indicates the reaction's progress. The observed redshifting from 430 after adding reducing agent to 447 nm after 4 h of the reaction indicates increasing NPs size. The position of the maximum SPR band after a long time of

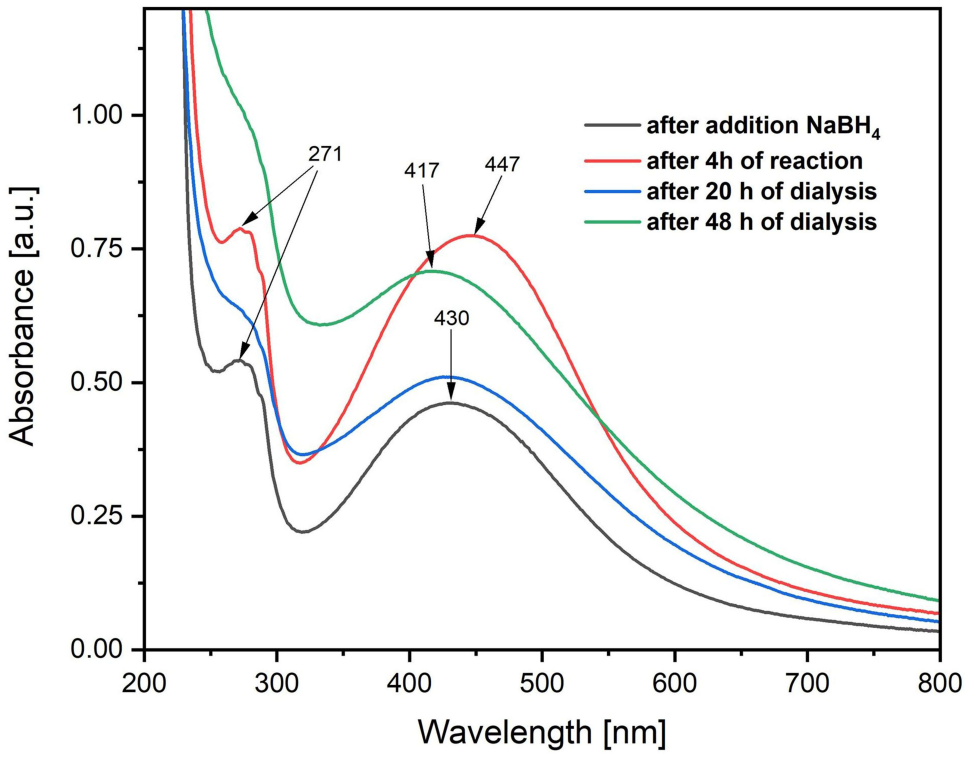

Figure 1 UV-vis spectra recorded during synthesis and purification of AgNPs-EPI. The bands with a maximum at 271 nm correspond to eptifibatide, and the bands with a maximum >400 nm correspond to surface plasmon resonance AgNPs.

dialysis (48 h) detected at 417 nm indicates that the NPs diameter is about 10 nm, which is consistent with results obtained from TEM analyses. The effectivity of dialysis in removing the excess of EPI's molecules not connected with nanoparticles surface is visible as decreasing the band's intensity with a maximum at 271 nm. The final product tested in all further experiments was obtained with the time of dialysis of 48 h to ensure that the synthesized material does not consist of eptifibatide molecules non-bounded with nanoparticles' surface.

Figure 2A shows a representative TEM image of the synthesized AgNPs-EPI and histogram 2 B with the size distribution of these nanoparticles. The synthesized NPs are spherical, narrow dispersive with an average diameter of metalcore 12.3 nm (more TEM images are presented in Supplementary Materials, Figure S1). Importantly, their propensity to self-assemble is detectable; they form groups of closely located objects that are not directly connected. Likely, molecules building organic layers on the surface of the NPs interact strongly via intermolecular interactions. This phenomenon may explain the results of DLS measurements. Compared with the average diameter of metal cores of the fabricated nanoparticles (from TEM measurements), their hydrodynamic diameters are surprisingly extensive, almost 200 nm (number size distribution). This difference may be explained based on the ability of the NPs to agglomerate via multidimensional interactions with amino acids building the peptide layer on their surface. Furthermore, the ability of amino acids to interact with water molecules via strong hydrogen interactions may also be responsible for the thick solvation shell forming around the NPs. The determined negative sign of zeta potential for the NPs shows that the functional groups in the protecting layer are ionized (mostly carboxylic groups); thus, the interactions with water molecules are more potent than in the case of neutral groups.

Figure 3 displays FTIR spectra recorded for the conjugate of silver nanoparticles with eptifibatide (AgNPs-EPI) and for this compound when it is non-bonded to the nanoparticles' surface (EPI). The characteristic bands corresponding to functional groups in the drug molecule appear in the AgNPs-EPI spectrum. The maxima of bands are located at the exact value of the wavenumber or shifted. Due to the presence of many functional groups (amine, carbonyl and amide) interacting mainly via hydrogen bonding groups, broadening the bands are observed in both spectra. The band

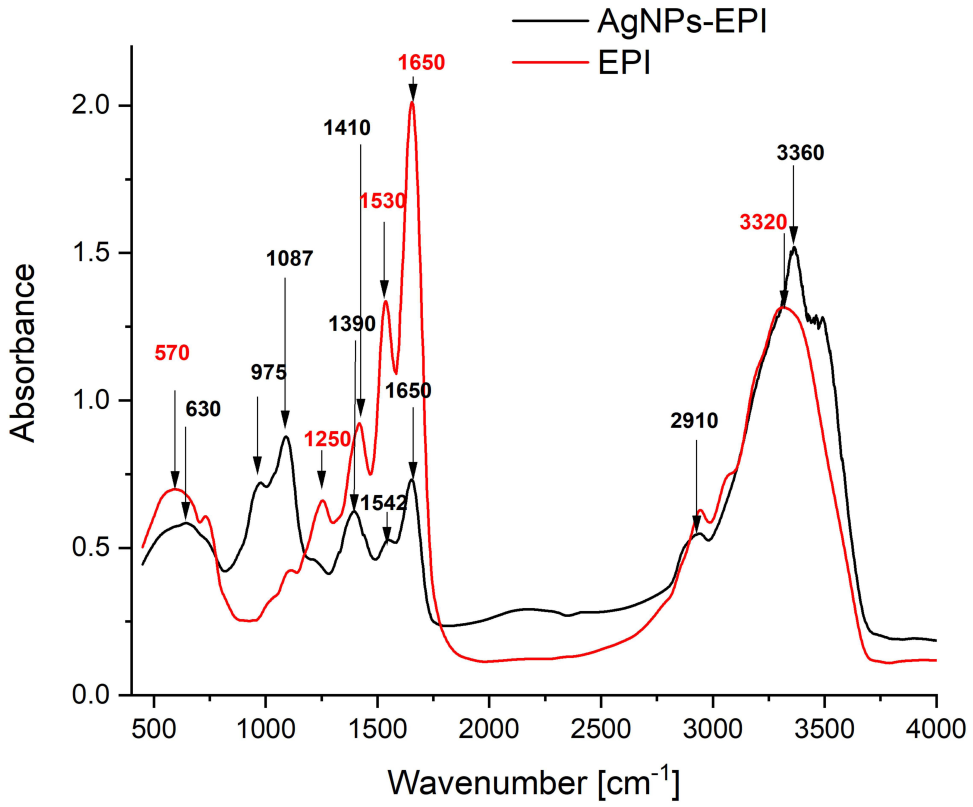

Figure 2 A representative TEM image of AgNPs-EPI (**A**) a histogram of size distribution obtained from the image: (**B**) and the results of DLS measurements: (**C**).

corresponding to the disulphide group appears at 570 cm^{-1} in the EPI molecule; meanwhile, in the conjugate spectrum, the band is significantly shifted to a higher wavelength with a maximum at 630 nm. The formation of the silver-sulphur bonds can explain it.[25] The most intensive bands in both spectra correspond to amine and amide groups. The vibration mode for amide carbonyl C=O bonds appears at 1650 cm^{-1} for both conjugate and free EPI molecules. It indicates a lack of interactions between these groups with the silver surface. However, the bands corresponding to C-N amide bonds (1530 and 1250 cm^{-1} in the EPI spectrum) are shifted in the AgNPs-EPI spectrum to lower wavenumbers. It suggests constraining these groups' motions in the conjugate, probably due to their interactions with silver (via nitrogen atoms). N-H stretch peaks characteristic of secondary amines at 3300 cm^{-1} are very strong in both spectra and located very close. Generally, the FTIR spectrum recorded for AgNPs-EPI confirmed the presence of the same functional groups as in EPI molecules, which means that they have not been transformed during the conjugate synthesis. Notably, the formation of Ag-S bonds between EPI molecule and nanoparticle's surface can also be observed in the FTIR spectrum.

Thermal gravimetric analyses (TGA) allowed for determining silver content in the synthesized NPs. Figure 4 shows TGA curves recorded for EPI and AgNPs-EPI. EPI decomposes in three steps (with maxima at 228°C, 320°C, and 711° C), and the process was completed at 800°C. In the case of AgNPs-EPI, decomposition of the organic fraction also occurs in three steps but at higher temperatures. Firstly, we observe that the drug connected with the metal core is more thermal stable than that not-connected, and it is a consequence of Ag-S bonds between the drug's molecules and nanoparticles. The final mass after decomposition of the organic fraction indicates that the content of silver is 29%, and the remaining EPI is 71%.

Assessment of Biocompatibility

The MTT and LDH assays were used to measure the viability of HMEC-1 cells and platelets following exposure to AgNPs-EPI (1–125 µg/mL). As shown in Figure 5, the viability of HMEC-1 was decreased only at 125 µg/mL.

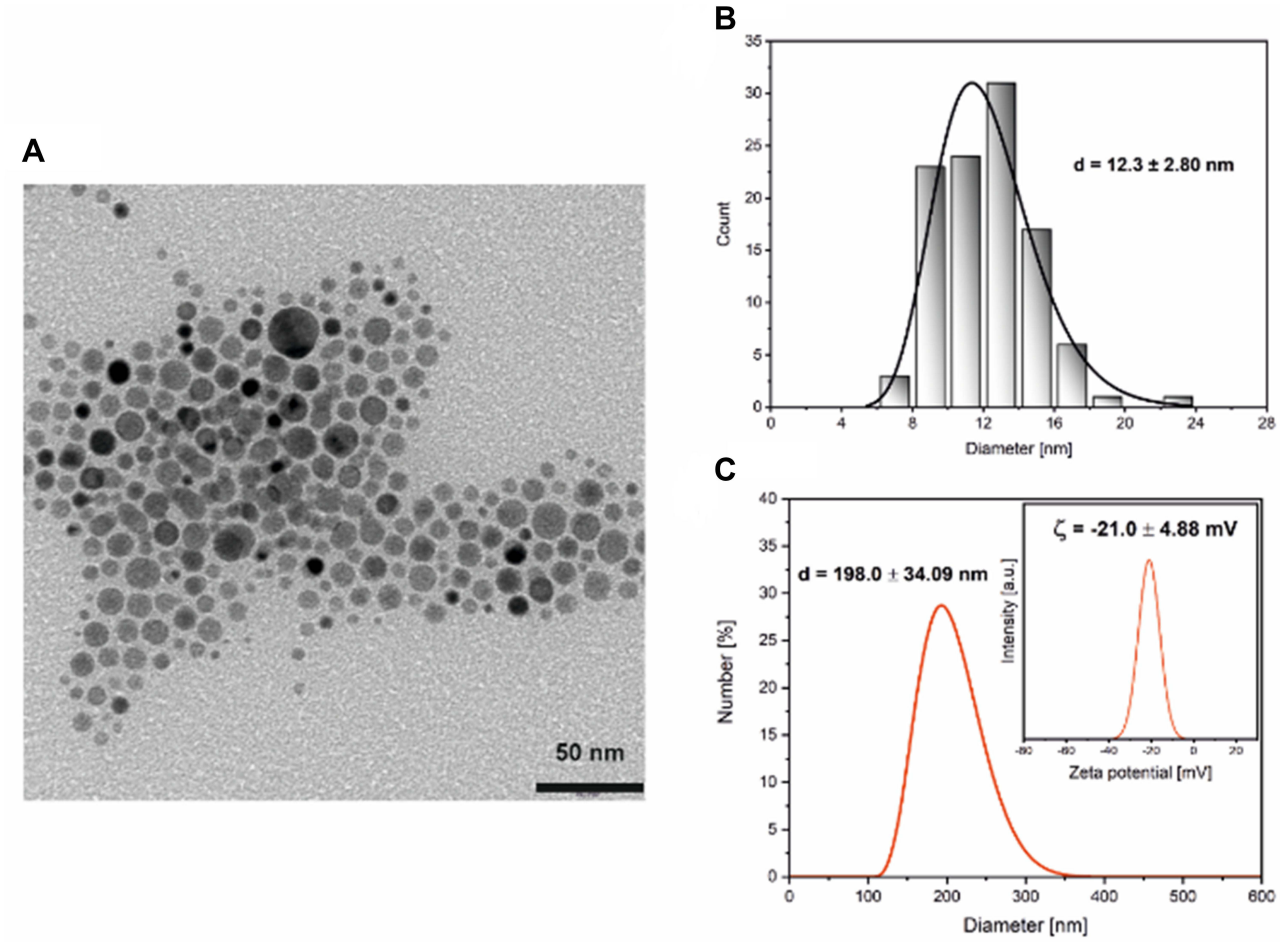

Figure 3 FTIR spectra recorded for synthesized conjugate and eptifibatide not bound with nanoparticles (samples prepared as pellets with KBr in a ratio of 1:200 (w/w)).

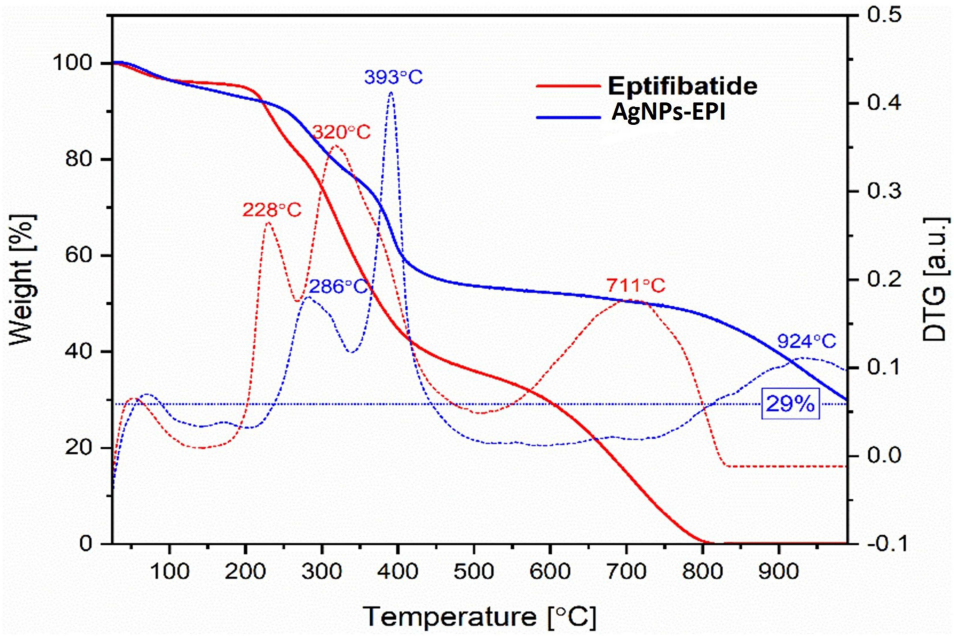

Figure 4 TGA curves recorded for AgNPs-EPI and eptifibatide (solid lines) and corresponding derivatives with temperature (dotted lines).

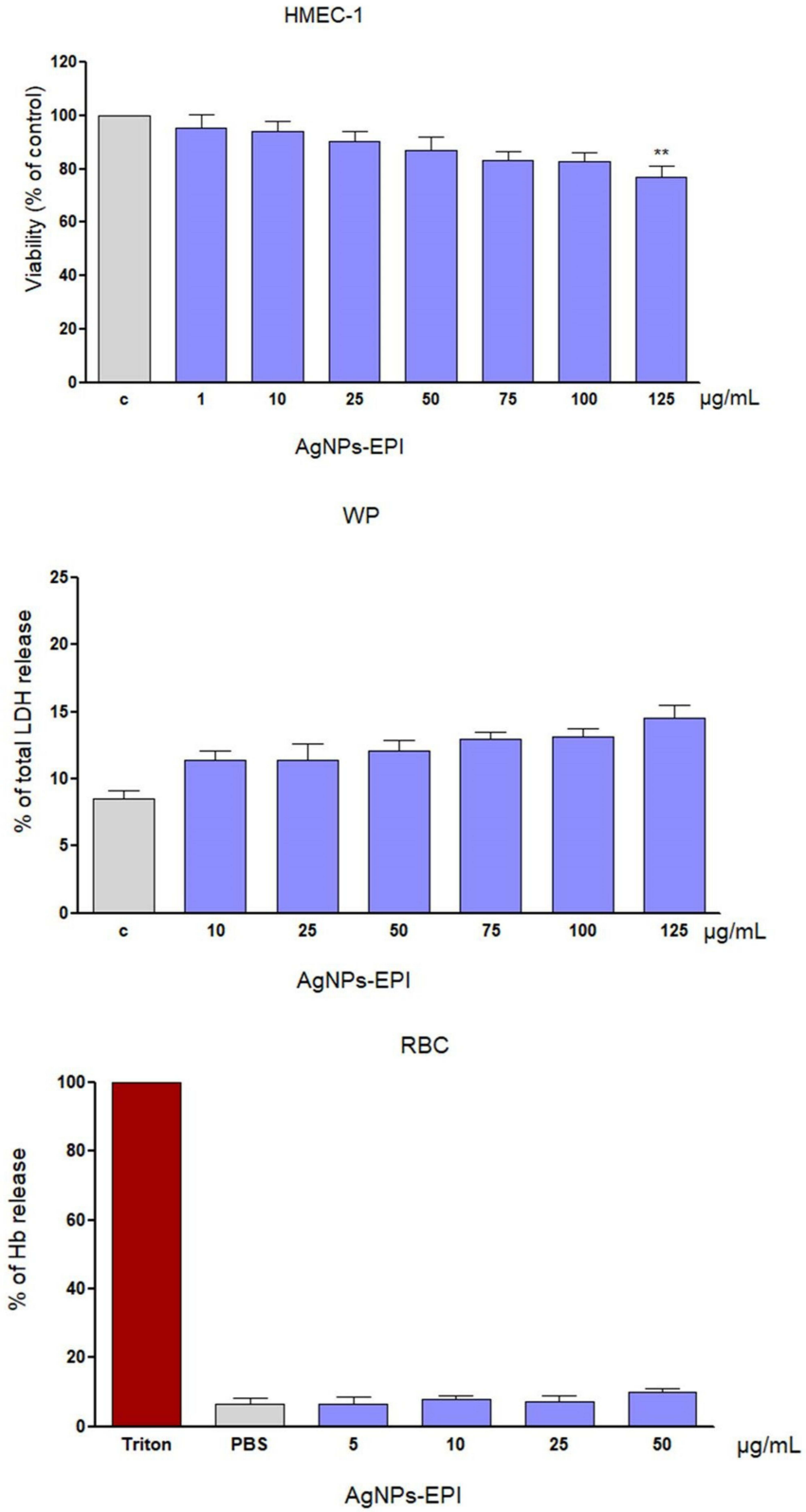

Figure 5 Effects of AgNPs-EPI on washed platelets (WP), endothelial cells (HMEC-1) viability following 24 h incubation and % Hb release from RBCs after 12 h incubationData are mean ±SD, n = 3. **p < 0.01.

Moreover, AgNPs-EPI did not induce significant hemolysis leading to ~10% of Hb at the highest concentration tested (50 µg/mL).

Inhibition of Collagen-Induced Washed Platelet (WP) Aggregation by AgNPs-EPI and EPI Under Stirring

Figure 6 shows the effects of AgNPs-EPI and EPI on collagen-induced platelet aggregation. Both compounds inhibited aggregation concentration-dependent; however, AgNPs-EPI were more potent than EPI, with IC_{50}= 14 and 23.4 for AgNPs-EPI and EPI, respectively.

Flow-Induced Inhibition of Platelet Aggregation with AgNPs-EPI and EPI

Figure 7 shows that AgNPs-EPI significantly inhibited flow-induced platelet aggregation, as shown by increased closure time in collagen/ADP and collagen/epinephrine cartridges.

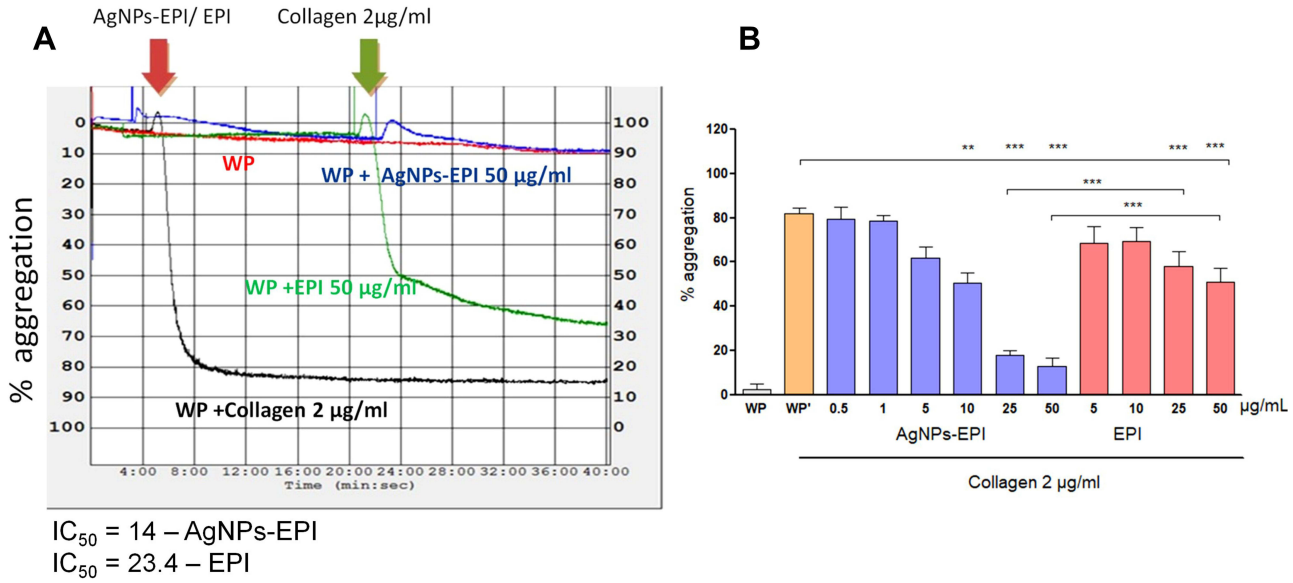

Figure 6 Inhibition of collagen-induced washed platelet (WP) aggregation by AgNPs-EPI and EPI, (**A**) – representative light aggregometry tracings showing the anti-aggregator effects of AgNPs-EPI and EPI both at 50 µg/mL. Collagen (black line) was used as a positive control; stirred platelets in the absence of NPs/drug were used as negative control (red line); platelet incubated with AgNPs-EPI with EPI (50µg/mL) and stimulated with collagen (blue line); platelet incubated with EPI (50µg/mL) and stimulated with collagen (green line). The brown arrow indicates the addition of NPs/drug, the green arrow indicates the addition of collagen. (**B**) – the statistical analysis of AgNPs-EPI and EPI effects on collagen-induced platelet aggregation. Data are mean ± standard deviation. **p < 0.001, ***p < 0.001 versus WP' (positive control).

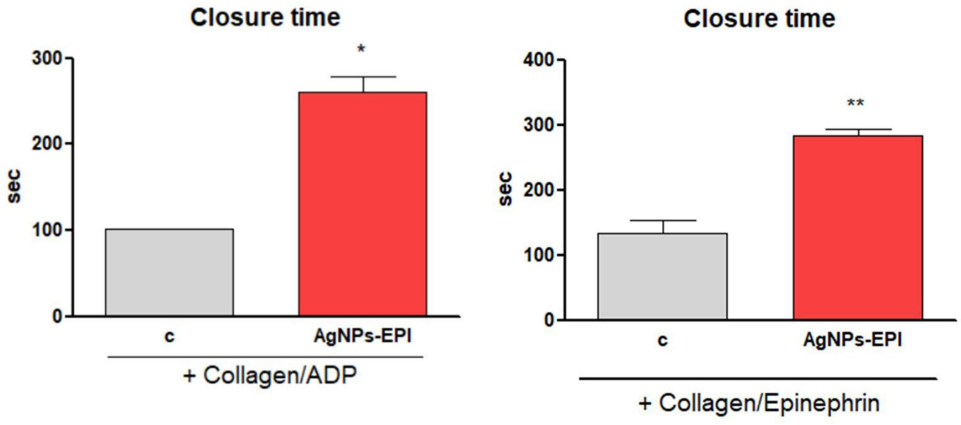

Figure 7 Inhibition flow-induced platelet aggregation with collagen/ADP and collagen/epinephrine cartridges by AgNPs-EPI, c – control closure time. Data are mean ±SD. *p < 0.05, **p < 0.005 versus control.

Effects of AgNPs-EPI and EPI on P-Selectin and GPIIb/IIIa Receptor Abundance

Figure 8 shows that both compounds concentration-dependently inhibited the abundance of P-selectin and GPIIb/IIIa on the platelet surface, and AgNPs-EP was more effective than EPI.

Effects of AgNPs-EPI on Platelet Mitochondrial Function

Figure 9A shows that activation of platelets by collagen resulted in a significant increase in LEAK respiration, an effect that was not significantly modified by AgNPs-EPI and EPI.

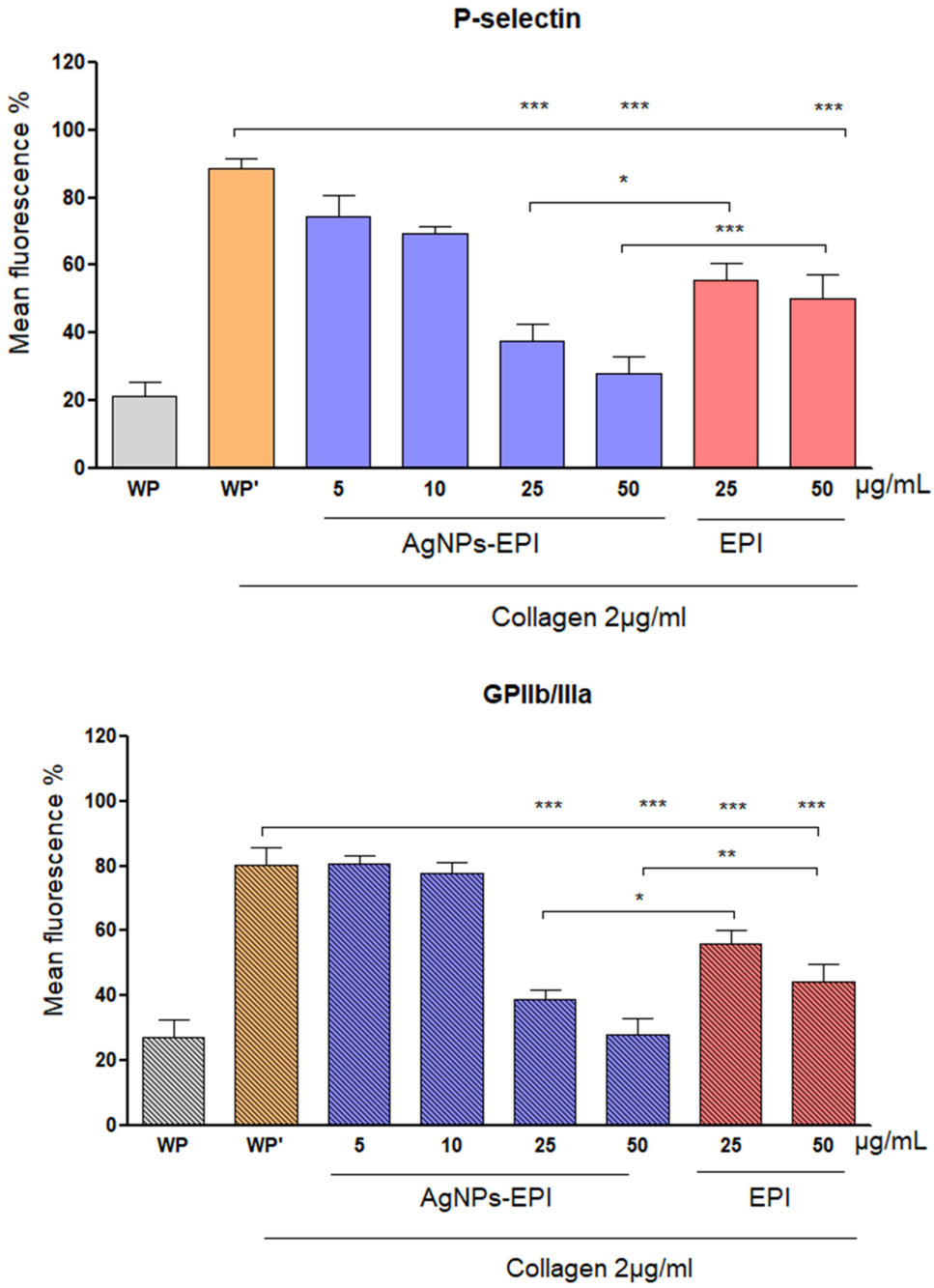

Figure 8 Inhibition of collagen-induced platelet receptor (GPIIb/IIIa and P-selectin) abundance by AgNPs-EPI and EPI. The statistical analysis of the effects of AgNPs-EPI and EPI. Data are expressed as mean ± standard deviation. *p < 0.05, **p < 0.001, ***p < 0.001 versus WP' (positive control).

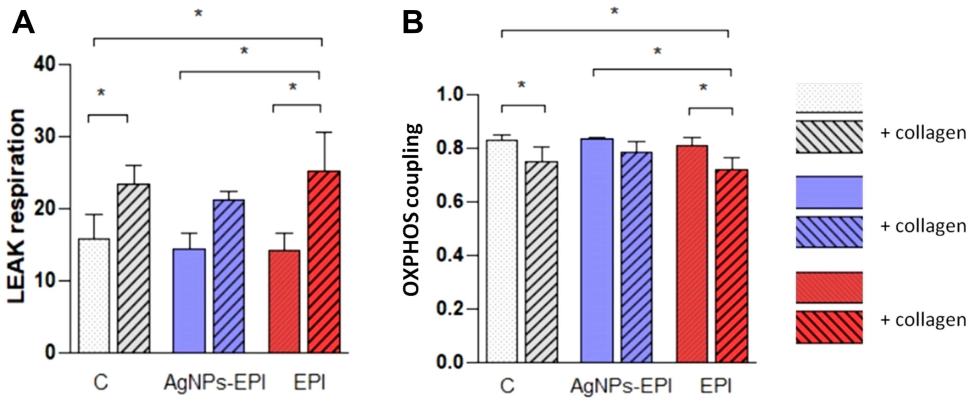

Figure 9 Effects of collagen-induced platelet aggregation on leak respiration (**A**) and OXPHOS coupling efficiency (**B**) in the presence or absence of AgNPs-EPI and EPI. Data are mean ±SD. *p < 0.05. Hatched bars show the effects of AgNPs-EPI and EPI in the presence of collagen (2 µg/mL).

In contrast, collagen resulted in a significant decrease in oxidative phosphorylation (OXPHOS) coupling efficiency. This effect was inhibited by AgNPs-EPI but not EPI (Figure 9B). Other respiration parameters (state CI, state CI + CII, state E, and state R) were not significantly changed (Table S1- Supplementary Materials).

Effects of AgNPs-EPI and EPI on the Secretion of Mediators by Endothelial Cells

The release of 6-keto-PGF1alpha, tPa, vWf, and cGMP from HMEC-1 cells was stimulated by thrombin. Figure 10 shows that AgNPs-EPI and EPI reduced the thrombin-induced release of these endothelial factors.

Coagulation System

The indices of the coagulation system (PT, APTT, APTT ratio, TT, INR, plasma fibrinogen, and D-dimers) were not significantly changed in the presence of AgNPs-EPI (Figure S2 -Supplementary Materials).

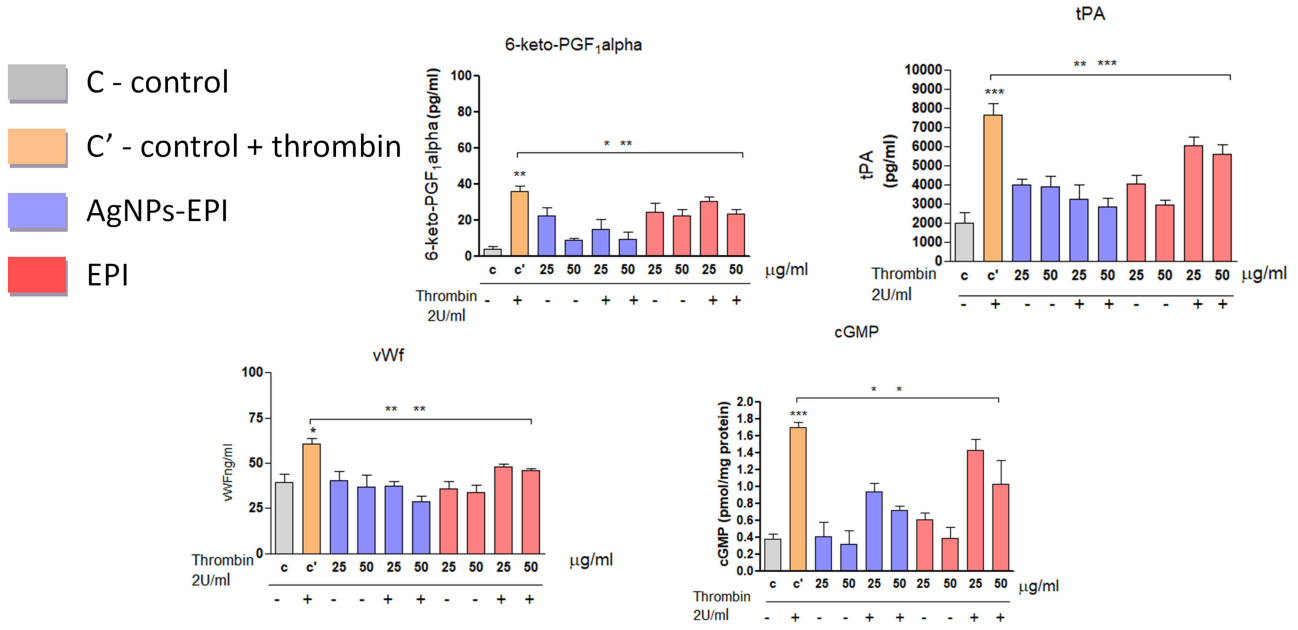

Figure 10 Inhibition of thrombin-induced release of 6-keto-PGF1alpha, tPA, vWF, and cGMP by AgNPs-EPI but not EPI. Preincubation of HMEC-1 cells with AgNPs-EPI inhibited the release of 6-keto-PGF1α, tPA, vWf, and cGMP. Data are mean ±SD. *p < 0.05, **p < 0.01, ***p < 0.001 to control or as indicated.

Discussion

This study aimed to synthesize and pharmacologically characterize AgNPs-EPI as a novel platelet aggregation inhibitor in vitro and ex vivo. We have found that: 1. AgNPs are an appropriate delivery platform for EPI, and 2. The synthesized AgNPs-EPI works as an effective inhibitor of platelet aggregation.

Pharmaceutical and Pharmacological Characterization of AgNPs-EPI

We have found that due to a disulfide bond in a molecule of EPI, it is possible to connect this drug to the nanosilver surface directly without any linker. According to this scheme, the chemisorption process of EPI on the AgNPs runs with the breaking of disulfide bonds. X-ray Photoelectron Spectroscopy and Electron Spin Resonance studies showed that the disulfide bonds could break onto the silver and gold surface during chemisorption and attached to the metal surface. [26–28] When designing a new pharmaceuticals based on silver nanoparticle platform, the potential cytotoxicity of silver nanomaterials should be taken into account.[29,30] The AgNPs-EPI synthesized for our experiments did not reduce the viability of human platelets and endothelial cells at concentrations<125 μg/mL, as shown by LDH and MTT tests. In addition, AgNPs-EPI tested in our work did not induce significant hemolysis when incubated with RBCs. Others and we have demonstrated that the cytotoxicity of AgNPs depends on the size, concentrations and functionalization of these materials.[31] As expected, the 12 nm AgNPs-EPI did not show significant cytotoxicity, similarly to the 2 nm AgNPs functionalized with glutathione, lipoic acid, or polyethylene glycol, as we have reported before.[32,33] Thus, AgNPs-EPI appear to be hemocompatible with endothelial cells, platelets and RBCs. We have then examined the pharmacological properties of AgNPs-EPI as a potential antiplatelet agent. There has been little research into the combination of eptifibatide and NPs. The encapsulation of the anticoagulant drug EPI in poly (DL-lactic-co-glycolic acid) (PLGA) nanoparticles was perfor med.[30] Experiments have shown effective drug delivery into the bloodstream and a low risk of platelet (membrane receptor) activation. Other researchers developed RGD-modified nanoliposomes (RGD-MNL) prepared as carriers for the targeted delivery of eptifibatide to activated platelets. The nanoliposomes had a size of about 10 nm, encapsulation efficiency of 37.5%, and good stability for 21 days, with little change in the size of the nanoliposomes. The results obtained in an ex vivo study showed that the antiplatelet activity of eptifibatide encapsulated nanoliposomes was higher compared to the free drug (81.63 vs 46.17% for RGD-MNL).[34] Other PC-based nanocapsules (2.8 × 1012) with encapsulated eptifibatide were incorporated into microfluidic blood perfusion tests and in vivo tail thrombosis and bleeding models. Shear-triggered delivery of eptifibatide in these nanocapsules selectively inhibited thrombus formation in vitro under conditions of stenosis and high shear flow above a shear rate of 1000 s^{-1}, leaving thrombus formation under the physiological conditions of shear rate.[35] Our earlier and other studies showed an inhibitory effect on platelet aggregation after stimulation.[18,36,37] Interestingly, new AgNPs-EPI synthesized by us inhibited aggregation more effectively than the free drug (10% vs 65% for AgNPs-EPI) under stirring and flow conditions (doubling closure time). This is not surprising as both AgNPs and EPI inhibit platelet aggregation as separate entities.[9,38] It should also be taken into account that silver nanoparticles have been shown to effectively inhibit integrin-dependent functional platelet responses such as aggregation, secretion, adhesion to immobilized fibrinogen or collagen, and the retraction of the fibrin clot in a dose-dependent manner irrespective of the nature of the agonists used. In vivo studies in mouse models also supported the antiplatelet effect properties of nanosilver, suggesting its additive effect on platelet inhibition.[39] For this reason and the available research data, it is believed that in the case of AgNPs-EPI, the drug EPI enhances the antiplatelet effect of conjugated AgNPs.Moreover, as functionalized AgNPs form less nanoparticle aggregates than uncoated NPs this property could also contribute to mechanisms that underlie the platelet-inhibitory activity of these possibilities.[18] The closure time, measured with the Platelet Function Analyzer (PFA-100/200®), is now used as the measurement of bleeding time. This is a system that simulates the vessel wall under physiological shear stress conditions.[40] Furthermore, closure time has some clinical utility in the exclusion/detection of primary hemostatic disorders and is sometimes referred to as an "in vitro" bleeding time.[41] These results confirm that AgNPs-EPI inhibits flow-induced platelet aggregation.

To study the mechanism(s) of AgNPs-EPI-induced inhibition of platelet aggregation, we first investigated the effects of this nanomaterial on platelet energy metabolism as mitochondria are often targeted by nanosystems.[42]

Despite the low mitochondria count in platelets (5–8 mitochondria per platelet), these organelles play an essential role during platelet activation. The mitochondrial pathway of platelet activation includes increased mitochondrial reactive oxygen species (ROS) formation, calcium release, or collapse of membrane potential.[43] Indeed, stimulation of platelets with collagen leads to mitochondrial ROS generation and increased intraplatelet calcium levels.[44] Our results confirmed this observation. We observed that collagen stimulates platelet mitochondria LEAK respiration, related to the leak of H^+, and may be considered a factor corresponding to ROS generation.[45] Additionally, the mitochondrial coupling efficiency is also reduced by collagen. Interestingly, preincubation of platelets with AgNPs-EPI alleviated these changes, contributing to the inhibition of platelet aggregation. The second, and likely the major, mechanism underlying the inhibitory activity of AgNPs-EPI on platelet aggregation is this nanoparticle-drug construct's ability to inhibit the activation and/or function of GPIIb/IIIa receptor by flow cytometry studies. We also investigated the impact of AgNPs-EPI on HMEC-1 endothelial cells derived from blood vessels.[46] We have shown that, as expected, HMEC-1 cells, when stimulated by thrombin, release a panel of antithrombotic factors such as 6-keto-PGF1alpha cyclic GMP and tPA as well as prothrombotic factors including vWf, 6-keto-PGF1alpha is the stable metabolite of PGI_2 (prostaglandin I_2), which is potent vasodilator and inhibitor of platelet aggregation and a significant product of arachidonic acid metabolism in endothelial cells that are derived from large blood vessels.[47]

Endothelium-dependent vasorelaxation mediated by nitric oxide (NO) release is stimulated by a number of blood-borne factors, including thrombin. It has been proven that thrombin is one of the mediators of the coagulation process, and its presence causes the release of these factors from the endothelial structures.[20,48] The nitric oxide-cGMP pathway is known to have vasoprotective, platelet-inhibitory, anti-inflammatory, and antioxidant effects on the vascular wall.[49] The drugs aimed at increasing the level of cGMP in the pulmonary vascular system are highly therapeutically effective.[50] Endothelial cells are thought to be the main source of plasma t-PA, a major fibrinolytic agent that limits the progression of occlusive thrombi. In cultured endothelial cells, t-PA synthesis is up-regulated in response to thrombin, which we have confirmed in our studies.[36] On the other hand, treatment of endothelial cells with thrombin causes an immediate increase in phospholipid methylation which ultimately leads to the release of von Willebrand factor (vWF).[51] Upon vascular damage leading to the exposure of subendothelial structures, vWF rapidly binds to GPIb alpha receptor on platelets facilitating platelet adhesion and thrombus formation.[52] The vWF derived from coronary endothelial cells is significantly increased in the event of damage to the coronary artery, which indicates the pathogenetic role of vWF in cardio-thrombotic diseases.[53] In addition, high vWF levels have been shown to be prognostic in patients with ischemic heart disease, peripheral vascular disease, and inflammatory vascular disease.[54] Importantly, we have shown that AgNPs-EPI, contrary to free drugs, effectively counteract the release of vWF.This would effectively decrease platelet-subendothelium interactions and work towards the preservation of vascular integrity. However, the impact of down-regulation of the release of endothelial mediators such as tPA nitric oxide and prostacyclin on these interactions needs to be determined. The results confirm that AgNPs-EPI acts as a novel inhibitor of platelet and endothelial cell activation and can be used as a platform for drug delivery in cardiovascular diseases and for coating medical devices. In addition, in a physiological environment, endothelial cells are exposed to shear stresses that are induced by blood flow and its viscosity. It is necessary to use models that mimic more physiological conditions, such as flow-through experiments, that would provide better results for the effects of AgNPs-EPI on cells under near physiological conditions. Nano-drugs with anticoagulant potential may have specific effects, but importantly, many of the cardiovascular coagulation factors will be affected and significant interactions may occur, potentially disrupting the haemostatic balance unintentionally, which may lead to thrombosis or bleeding complications.[55] ConclusionWe designed, synthesized and characterized new AgNPs conjugates with eptifibatide. In vitro pharmacological profile analysis of this conjugate shows that it is effective in inhibiting human platelet aggregation and thrombin-induced endothelial activation at concentrations that do not affect cell viability. Moreover, AgNPs-EPI effects thrombin-induced endothelial activation factors such as 6-keto-PGF1alpha, tPA, vWF, and cGMP, which are associated with platelet aggregation, fibrin production, and occlusive thrombus formation, which is essential to prevent vascular damage and maintaining blood flow. Despite significant preclinical data showing that nanoanticoagulants may have a specific effect, it should be noted that many clotting factors will be encountered in the circulatory system and may interact with them, potentially disrupting the haemostatic balance inadvertently, which potentially lead to thrombosis or bleeding complication. An in-depth understanding of the interface between NPs and the coagulation system is valuable for the engineering and successful translation of NPs into the clinical trials and they could be potentially used to coat medical devices such as vascular catheters. Thus, it is appropriate to move AgNPs-EPI to further stages of preclinical development.

Abbreviations

AgNPs-EPI, silver nanoparticles with eptifibatide; APTT, activated partial thromboplastin time; cGMP, guanosine monophosphate cyclic; CT, closure time; DLS, dynamic light scattering; EPI, eptifibatide; HMEC-1, immortalized human microvascular endothelial cell line; LDH, lactate dehydrogenase; NPs, nanoparticles; PGI_2, prostacyclin; PT, prothrombin time; TEM, transmission electron microscopy; TGA, thermogravimetric analyses; tPA, tissue plasminogen activator; TT, thrombin time; WP, washed platelet.

Acknowledgments

This work was supported by grant HARMONIA (2017/26/M/NZ7/01030) from the Polish National Science Center (NCN).

Disclosure

The authors report no conflicts of interest in this work.

References

1. Yau JW, Teoh H, Verma S. Endothelial cell control of thrombosis. *BMC Cardiovasc Disord*. 2015;15(1):1–11. doi:10.1186/s12872-015-0124-z
2. Mackman N. Triggers, targets and treatments for thrombosis. *Nature*. 2008;451(7181):914–918. doi:10.1038/nature06797
3. Mackman N. New insights into the mechanisms of venous thrombosis. *J Clin Invest*. 2012;122(7):2331–2336. doi:10.1172/JCI60229
4. Everett LA, Cleuren ACA, Khoriaty RN, Ginsburg D. Murine coagulation factor VIII is synthesized in endothelial cells. *Blood*. 2014;123 (24):3697–3705. doi:10.1182/blood-2014-02-554501
5. Furie B, Furie BC. Mechanisms of thrombus formation. Mechanisms of disease. *N Engl J Med*. 2008;359(9):938–949. doi:10.1056/NEJMra0801082
6. Thachil J. Antiplatelet therapy-a summary for the general physicians. *Clin Med J R Coll Physicians*. 2016;16(2):152–160. doi:10.7861/clinmedicine.16-2-152
7. Ghoshal K, Bhattacharyya M. Overview of platelet physiology: its hemostatic and nonhemostatic role in disease pathogenesis. *Sci World J*. 2014;2014:1–16. doi:10.1155/2014/781857
8. Heitzer T, Ollmann I, Köke K, et al. Platelet glycoprotein IIb/IIIa receptor blockade improves vascular nitric oxide bioavailability in patients with coronary artery disease. *Circulation*. 2003;108(5):536–541. doi:10.1161/01.CIR.0000081774.31064.62
9. O'Shea JC, Tcheng JE. Eptifibatide: a potent inhibitor of the platelet receptor integrin, glycoprotein IIb/IIIa. *Expert Opin Investig Drugs*. 1999;8 (11):1893–1905. doi:10.1517/13543784.8.11.1893
10. Zhou X, Wu X, Sun H, Li J. Efficacy and safety of eptifibatide versus tirofiban in acute coronary syndrome patients: a systematic review and meta-analysis. *J Evid Based Med*. 2017;10(2):136–144. doi:10.1111/jebm.12253
11. Marmur JD, Poludasu S, Lazar J, Cavusoglu E. Long-term mortality after bolus-only administration of Abciximab, eptifibatide, or tirofiban during percutaneous coronary intervention. *Catheter Cardiovasc Interv*. 2009;73(2):214–221. doi:10.1002/ccd.21773
12. Fuentes E, Yameen B, Bong SJ, et al. Antiplatelet effect of differentially charged PEGylated lipid-polymer nanoparticles. *Nanomed Nanotechnol Biol Med*. 2017;13(3):1089–1094. doi:10.1016/j.nano.2016.10.010
13. Mathur P, Jha S, Ramteke S, Jain NK. Pharmaceutical aspects of silver nanoparticles. *Artif Cells Nanomedicine Biotechnol*. 2018;46(1):115–126. doi:10.1080/21691401.2017.1414825
14. Prasher P, Sharma M, Mudila H, et al. Emerging trends in clinical implications of bio-conjugated silver nanoparticles in drug delivery. *Colloids Interface Sci Commun*. 2020;35(December2019):100244. doi:10.1016/j.colcom.2020.100244
15. Niska K, Knap N, Kędzia A, et al. Capping agent-dependent toxicity and antimicrobial activity of silver nanoparticles: an in vitro study. concerns about potential application in dental practice. *Int J Med Sci*. 2016;13(10):772–782. doi:10.7150/ijms.16011
16. Zielinska E, Zauszkiewicz-Pawlak A, Wojcik M, Inkielewicz-Stepniak I. Silver nanoparticles of different sizes induce a mixed type of programmed cell death in human pancreatic ductal adenocarcinoma. *Oncotarget*. 2018;9(4):4675–4697. doi:10.18632/oncotarget.22563
17. Steckiewicz KP, Zwara J, Jaskiewicz M, et al. Shape-depended biological properties of Ag 3 PO 4 microparticles: evaluation of antimicrobial properties and cytotoxicity in in vitro model—safety assessment of potential clinical usage. *Oxid Med Cell Longev*. 2019;2019:1–19. doi:10.1155/2019/6740325
18. Hajtuch J, Hante N, Tomczyk E, et al. Effects of functionalized silver nanoparticles on aggregation of human blood platelets. *Int J Nanomedicine*. 2019;14:7399–7417. doi:10.2147/IJN.S213499
19. Qing Y, Cheng L, Li R, et al. Potential antibacterial mechanism of silver nanoparticles and the optimization of orthopedic implants by advanced modification technologies. *Int J Nanomedicine*. 2018;13:3311–3327. doi:10.2147/IJN.S165125
20. Sato T, Sawada S, Tsuda Y, et al. The mechanism of thrombin-induced prostacyclin synthesis in human endothelial cells with reference to the gene transcription of prostacyclin-related enzymes and Ca2+ kinetics. *J Pharmacol Toxicol Methods*. 1999;41(4):173–182. doi:10.1016/S1056-8719(99)00039-8
21. Radomski M, Moncada S. An improved method for washing of human platelets with prostacyclin. *Thromb Res*. 1983;30(4):383–389. doi:10.1016/0049-3848(83)90230-X
22. Bețiu AM, Chamkha I, Gustafsson E, et al. Cell permeable succinate rescues mitochondrial respiration in cellular models of amiodarone toxicity. *Int J Mol Sci*. 2021;22(21):11786. doi:10.3390/ijms222111786
23. Figueira TR, Melo DR, Vercesi AE, Castilho RF. Computational modeling of mitochondrial function. In:*Mitochondrial Bioenergetics*. Vol. 810. Humana Press; 2012. doi:10.1007/978-1-61779-382-0

24. Stegemann A, Flis D, Ziolkowski W, et al. The α7 nicotinic acetylcholine receptor: a promising target for the treatment of fibrotic skin disorders. *J Invest Dermatol*. 2020;140(12):2371–2379. doi:10.1016/j.jid.2020.04.006
25. Tripathy SK, Yu YT. Spectroscopic investigation of S-Ag interaction in ω-mercaptoundecanoic acid capped silver nanoparticles. *Spectrochim Acta*. 2009;72(4):841–844. doi:10.1016/j.saa.2008.12.004
26. Megiel E. Surface modification using TEMPO and its derivatives. *Adv Colloid Interface Sci*. 2017;250:158–184. doi:10.1016/j.cis.2017.08.008
27. Gozdziewska M, Cichowicz G, Markowska K. Nitroxide-coated silver nanoparticles: synthesis, surface physicochemistry and antibacterial activity. *J Mater Chem C*. 2015;3:10715–10722. doi:10.1039/b000000x
28. Swiech O, Bilewicz R, Megiel E. TEMPO coated Au nanoparticles: synthesis and tethering to gold surfaces. *RSC Adv*. 2013;3(17):5979–5986. doi:10.1039/c3ra23106b
29. Akter M, Sikder MT, Rahman MM, et al. A systematic review on silver nanoparticles-induced cytotoxicity: physicochemical properties and perspectives. *J Adv Res*. 2018;9:1–16. doi:10.1016/j.jare.2017.10.008
30. Steckiewicz KP, Cieciórski P, Barcińska E, et al. Silver nanoparticles as chlorhexidine and metronidazole drug delivery platforms: their potential use in treating periodontitis. *Int J Nanomedicine*. 2022;17:495–517. doi:10.2147/IJN.S339046
31. Perde-Schrepler M, Florea A, Brie I, et al. Size-dependent cytotoxicity and genotoxicity of silver nanoparticles in cochlear cells in vitro. *J Nanomater*. 2019;2019:1–13. doi:10.1155/2019/6090259
32. Hajtuch J, Santos-Martinez MJ, Wojcik M, et al. Lipoic acid-coated silver nanoparticles: biosafety potential on the vascular microenvironment and antibacterial properties. *Front Pharmacol*. 2022;12:1–13. doi:10.3389/fphar.2021.733743
33. Barcińska E, Wierzbicka J, Zauszkiewicz-Pawlak A, et al. Role of oxidative and nitro-oxidative damage in silver nanoparticles cytotoxic effect against human pancreatic ductal adenocarcinoma cells. *Oxid Med Cell Longev*. 2018;2018:15. doi:10.1155/2018/8251961
34. Bardania H, Shojaosadati SA, Kobarfard F, et al. Encapsulation of eptifibatide in RGD-modified nanoliposomes improves platelet aggregation inhibitory activity. *J Thromb Thrombolysis*. 2017;43(2):184–193. doi:10.1007/s11239-016-1440-6
35. Molloy CP, Yao Y, Kammoun H, et al. Shear-sensitive nanocapsule drug release for site-specific inhibition of occlusive thrombus formation. *J Thromb Haemost*. 2017;15(5):972–982. doi:10.1111/jth.13666
36. Dakshayani SS, Marulasiddeshwara MB, Sharath SK, et al. *Antimicrobial, Anticoagulant and Antiplatelet Activities of Green Synthesized Silver Nanoparticles Using Selaginella (Sanjeevini) Plant Extract*. Vol. 131. Elsevier B.V; 2019. doi:10.1016/j.ijbiomac.2019.01.222
37. Marulasiddeshwara MB, Dakshayani SS, Sharath Kumar MN, et al. Facile-one pot-green synthesis, antibacterial, antifungal, antioxidant and antiplatelet activities of lignin capped silver nanoparticles: a promising therapeutic agent. *Mater Sci Eng C*. 2017;81:182–190. doi:10.1016/j.msec.2017.07.054
38. Hante NK, Medina C, Santos-Martinez MJ. Effect on platelet function of metal-based nanoparticles developed for medical applications. *Front Cardiovasc Med*. 2019;6. doi:10.3389/fcvm.2019.00139
39. Shrivastava S, Bera T, Singh SK, et al. Characterization of antiplatelet properties of silver nanoparticles. *ACS Nano*. 2009;3(6):1357–1364. doi:10.1021/nn900277t
40. Favaloro EJ. The Platelet Function Analyser (PFA)-100 and von Willebrand disease: a story well over 16 years in the making. *Haemophilia*. 2015;21(5):642–645. doi:10.1111/hae.12710
41. Hayward CPM, Harrison P, Cattaneo M, et al. Platelet function analyzer (PFA)-100® closure time in the evaluation of platelet disorders and platelet function: reply to a rebuttal. *J Thromb Haemost*. 2006;4(6):1433–1434. doi:10.1111/j.1538-7836.2006.01992.x
42. Lopez JJ, Salido GM, Pariente JA, Rosado JA. Thrombin induces activation and translocation of Bid, Bax and Bak to the mitochondria in human platelets. *J Thromb Haemost*. 2008;6(10):1780–1788. doi:10.1111/j.1538-7836.2008.03111.x
43. Melchinger H, Jain K, Tyagi T, Hwa J. Role of platelet mitochondria: life in a nucleus-free zone. *Front Cardiovasc Med*. 2019;6:1–11. doi:10.3389/fcvm.2019.00153
44. Yamagishi SI, Edelstein D, Du XL, Brownlee M. Hyperglycemia potentiates collagen-induced platelet activation through mitochondrial superoxide overproduction. *Diabetes*. 2001;50(6):1491–1494. doi:10.2337/diabetes.50.6.1491
45. Brookes PS. Mitochondrial H + leak and ROS generation: an odd couple. *Free Radic Biol Med*. 2005;38(1):12–23. doi:10.1016/j.freeradbiomed.2004.10.016
46. Muñoz-Vega M, Massó F, Páez A, et al. Characterization of immortalized human dermal microvascular endothelial cells (HMEC-1) for the study of HDL functionality. *Lipids Health Dis*. 2018;17(1):1–8. doi:10.1186/s12944-018-0695-7
47. Charo IF, Shak S, Karasek MA, Davison PM, Goldstein IM. Prostaglandin I2 is not major metabolite of arachidonic acid in cultured endothelial cells from human foreskin microvessels. *J Clin Invest*. 1984;74(3):914–919. doi:10.1172/JCI111509
48. Zhang A, Hou Y, Sun C, et al. Baicalin protects against thrombin-induced cell injury in human umbilical vein endothelial cells. *Bio Med Res Int Bind*. 2019;2019. doi:10.1155/2019/7405602
49. Nickel KF, Laux V, Heumann R, von Degenfeld G. Thrombin has biphasic effects on the nitric oxide-cGMP pathway in endothelial cells and contributes to experimental pulmonary hypertension. *PLoS One*. 2013;8(6):e63504. doi:10.1371/journal.pone.0063504
50. Nagaya N, Uematsu M, Oya H, et al. Short-term oral administration of L-arginine improves hemodynamics and exercise capacity in patients with precapillary pulmonary hypertension. *Am J Respir Crit Care Med*. 2001;163(4):887–891. doi:10.1164/ajrccm.163.4.2007116
51. Suchen LH, Ching-ying NJM, Patton TGG, Patton G. Prostacyclin synthesis and deacylation of phospholipids in endothelial cells: comparison of thrombin, histamine and ionophore A23187. *Thromb Res*. 1985;38(1):1–10. doi:10.1016/0049-3848(85)90002-7
52. Peyvandi F, Garagiola I, Baronciani L. Role of von Willebrand factor in the haemostasis. *Blood Transfus*. 2011;9:3–8. doi:10.2450/2011.002S
53. Fan M, Wang X, Peng X, et al. Prognostic value of plasma von Willebrand factor levels in major adverse cardiovascular events: a systematic review and meta-analysis. *BMC Cardiovasc Disord*. 2020;20(1):1–9. doi:10.1186/s12872-020-01375-7
54. Lip GYH, Blann A. von Willebrand factor: a marker of endothelial dysfunction in vascular disorders? *Cardiovasc Res*. 1997;34(2):255–265. doi:10.1016/S0008-6363(97)00039-4
55. Shurbaji S, Anlar GG, Hussein EA, et al. Effect of flow-induced shear stress in nanomaterial uptake by cells: focus on targeted anti-cancer therapy. *Cancers*. 2020;12(7):1–16. doi:10.3390/cancers12071916